Evaluation of Upper Airway Collapsibility Using Real-Time MRI

Ziyue Wu PhD,[1,2]* Weiyi Chen MS,[3] Michael C.K. Khoo PhD,[1]
Sally L. Davidson Ward MD,[4] and Krishna S. Nayak PhD[1,3]

Purpose: To develop and demonstrate a real-time MRI method for assessing upper airway collapsibility in sleep apnea.
Materials and Methods: Data were acquired on a clinical 3 Tesla scanner using a radial CAIPIRIHNA sequence with modified golden angle view ordering and reconstructed using parallel imaging and compressed sensing with temporal finite difference sparsity constraint. Segmented airway areas together with synchronized facemask pressure were used to calculate airway compliance and projected closing pressure, P_{close}, at four axial locations along the upper airway. This technique was demonstrated in five adolescent obstructive sleep apnea (OSA) patients, three adult OSA patients and four healthy volunteers. Heart rate, oxygen saturation, facemask pressure, and abdominal/chest movements were monitored in real-time during the experiments to determine sleep/wakefulness.
Results: Student's t-tests showed that both compliance and P_{close} were significantly different between healthy controls and OSA patients ($P < 0.001$). The results also suggested that a narrower airway site does not always correspond to higher collapsibility.
Conclusion: With the proposed methods, both compliance and P_{close} can be calculated and used to quantify airway collapsibility in OSA with an awake scan of 30 min total scan room time.

J. MAGN. RESON. IMAGING 2016;44:158–167.

Sleep apnea is a common disorder characterized by repetitive pauses in breathing or shallow breaths during sleep. Obstructive sleep apnea (OSA) is the most common type in which the apnea is caused by a physical collapse of pharyngeal airway.[1] Despite respiratory effort, the airway obstruction results in reduced or ceased gas exchange, followed by blood oxygen desaturation, resulting in frequent arousals during sleep. When untreated, OSA significantly decreases quality of life and workplace productivity, and increases the risk of traffic and workplace accidents and diseases such as heart attack,[2] stroke,[3] obesity,[4] and diabetes.[5] The total economic cost of OSA is estimated to be $150 billion per year in the United States, a figure much higher than the direct cost of diagnosing and treating sleep apneas ($2–10 billion per year).[6]

Airway collapse in OSA is typically attributed to excessive soft tissues (adenoids, tonsils, soft palate, tongue, and epiglottis) and/or increased airway collapsibility.[7,8] Obesity contributes to both of these factors and has been identified as a potent risk factor highly linked to OSA.[9] The prevalence of OSA has been reported to be 4–9% in adults and 2% in children,[10] and is likely to rise due in part to the worldwide obesity epidemic.[11]

The standard technique for assessing sleep apnea is polysomnography (PSG),[12,13] an overnight sleep study which records a comprehensive set of physiological signals. They include brain electrical activity (EEG), eye movement, blood oxygen saturation, heart rate, and respiratory effort, from which sleep disorders such as apneas can be identified. Apnea-Hypopnea Index (AHI), defined as the number of apnea events per hour, is used to grade the severity of sleep apnea.[14,15] Patients are typically diagnosed as having mild sleep apnea when they present an AHI of 5–14, moderate sleep apnea when they present an AHI of 15–30, and severe sleep apnea if AHI exceeds 30.[15] However, it has been shown that AHI alone does not adequately quantify the extent of the breathing disturbance.[16,17] AHI is based on indirect measurements and does not provide any anatomical information about the airway obstruction, nor does it

View this article online at wileyonlinelibrary.com. DOI: 10.1002/jmri.25133

Received Sep 16, 2015, Accepted for publication Dec 2, 2015.

*Address reprint requests to: Z.W., 28900 Fountain Parkway, Alltech Medical Systems America, Solon, OH 44139. E-mail: ziyuewu@usc.edu

From the [1]Department of Biomedical Engineering, University of Southern California, Los Angeles, California, USA; [2]Alltech Medical Systems America, Solon, Ohio, USA; [3]Ming Hsieh Department of Electrical Engineering, University of Southern California, Los Angeles, California, USA; and [4]Children's Hospital Los Angeles, Keck School of Medicine, University of Southern California, Los Angeles, California, USA

provide any quantitative properties that measure tissue collapsibility. Both of these are useful to the appreciation of the pathophysiology and to tailor treatment to individual patients.[18–22] Therefore, direct access of such information with an imaging tool is highly desired and attempts have been made using several modalities including fluoroscopy,[22,23] fiberoptic nasoendoscopy,[24–26] CT,[27–29] acoustic reflection,[30,31] and most recently optical coherence tomography (OCT)[32] and MRI.

Three-dimensional (3D) static MRI can generate excellent tissue contrast and identify potential anatomical risk factors and airway narrowing.[33,34] Enlarged airway tissues such as the adenoids and tonsils can be easily identified with T2 contrast and positive correlations have been found between OSA and these enlarged tissues. Tongue and neck fat are also risk factors that can be quantified using static MRI. CINE techniques have also been implemented to measure the changes of upper airway during tidal breathing.[21,35–38] Due to the acquisition speed constraints, data from multiple respiratory cycles are used to form one cycle of dynamic images based on respiratory gating in these methods.

The idea of using airway closing pressure to measure airway collapsibility in OSA originates in Issa and Sullivan.[39] Starting from the point at which the upper airway had been stabilized through application of continuous positive airway pressure (CPAP). By applying inspiratory occlusions at the mask, they found that peak inspiratory pressure (at the mask) and esophageal pressure (representing respiratory effort) became progressively more negative. At the point of upper airway closure, the negative excursions of mask pressure plateaued. Airway compliance has also been proposed as a metric for airway collapsibility,[40–42] and is defined as the change in airway cross-sectional area per unit of pressure.[24] Compliance testing involves the generation of negative pressure by means of brief inspiratory load (one to three breaths) during real-time imaging of a 2D axial slice. Under these conditions, airway motion can be rapid, requiring roughly 100 ms temporal and 1 mm spatial resolution.[43] The spatiotemporal resolution (1.95 mm, 667 ms) and single slice coverage[44] of conventional real-time MRI are inadequate. Alternative imaging schemes have been proposed, including 2D spiral (2.6 mm, 181 ms)[21] and EPI (1.56 mm, 160 ms),[45] interleaved multi-slice (1.6 mm/2000 ms/3-slice),[46] and 3D real-time imaging using compressed sensing (2 mm, 388 ms),[47] however, none of these approaches have provided adequate spatiotemporal resolution and coverage for airway compliance testing. Simultaneous-multi-slice (SMS) or 3D imaging that covers more of the relevant pharyngeal airway (i.e., from soft palate to epiglottis) would be a major advance as it would allow more comprehensive evaluation of possible collapsing sites along the pharyngeal airway.

The purpose of this work is to develop and demonstrate a real-time imaging method with adequate spatiotemporal resolution and coverage for assessing upper airway collapsibility in sleep apnea.

Materials and Methods

Experiment Setup

Experiments were performed on a 3 Tesla(T) GE Signa HDxt scanner (GE Healthcare, Waukesha, WI) with gradients capable of 40 mT/m amplitude and 150 mT/m/ms slew rate. A body transmission coil and a six-channel carotid receiver coil (NeoCoil, Pewaukee, WI) were used.

During the scan, a facemask (Hans Rudolph Inc., Kansas City, MO) that covers both nose and mouth was used for measurement of airway pressure and for creating an inspiratory load for compliance testing. Small-bore tubing from the mask port was connected to an MP-45 pressure transducer (Validyne Engineering Inc., Northridge, CA) for measurement of mask pressure. The inspiratory port of the mask was connected through an extension hose to an inflatable balloon valve (Model 9325, Hans Rudolph Inc., Shawnee, KS) that was used to control the flow of air entering the mask. The scan operator was able to initiate an inspiratory occlusion by pneumatically activating the balloon valve through an automated valve controller (Model 9330, Hans Rudolph Inc., Shawnee, KS), located in the MRI console room. The occlusion[45] served as external inspiratory load that could lead to substantial narrowing of the upper airway during inspiration. In addition, several other physiological signals were monitored and recorded during the MRI scan, as shown in Figure 1. An optical fingertip plethysmograph (Biopac Inc., Goleta, CA) was used to measure heart rate and oxygen saturation. A respiratory transducer (Biopac Inc., Goleta, CA) and the scanner's built-in respiratory bellows were used to measure respiratory effort at the lower chest and abdomen. The combined information of respiratory efforts (facemask pressure, chest/abdomen movements), heart rate, and oxygen saturation were monitored in real-time by a pediatric pulmonologist (2 years of experience) to determine sleep/wakefulness. Sleep was inferred from a lack of any movement artifact or other behavioral features associated with wakefulness such as swallowing and by the presence of minimal variation in heart rate and respiratory pattern consistent with sleep. Sleep was also confirmed by querying the subject after the MRI scan.

Five adolescent OSA patients (3M2F; age 13–17 years; 68–115 kg), three adult OSA volunteers (3M; age 30–40 years; 75–90 kg), and four healthy adult volunteers (2M2F; age 23–30 years; 47–83 kg) were studied. The experiment protocol was approved by the Institutional Review Boards of University of Southern California and Children's hospital Los Angeles, and informed consent was obtained from all subjects. Each recruited adolescent first underwent an overnight PSG which determined the severity of OSA in each subject. All adult OSA volunteers were previously diagnosed to have OSA (AHI $>$ 5) based on their PSG test results and were using CPAP treatment at the time of studies. All healthy volunteers reported that they had no sleep disorders and no excessive daytime sleepiness. The total time inside the scanner was 1 h for each adolescent OSA patient. All the adult OSA patients and volunteers were inside the scanner for 30 min and stayed awake. For the adolescent OSA patients, a total of three occlusions were induced in the first 10 min of the study when the subject was awake, with

FIGURE 1: Experimental setup for airway collapsibility measurement. Left: A facemask covering nose and mouth is connected to an external hose, which contains an inflatable balloon. Once expanded, the balloon can block the air flow and serve as external inspiratory load. Physiological signals including facemask pressure, chest and abdomen displacements, oxygen saturation, and heart rate are simultaneously recorded and synchronized with MRI acquisition. Right: Positioning of the six-channel receiver coil. Note that subjects in this study wore all equipment shown in both panels.

approximately 3 min interval. Another three occlusions were induced whenever the physiological signals indicated that the subject fell asleep, with at least 3-min interval. After that, another three occlusions were induced with 3-min interval when the subject was awake, or if the subject did not fall asleep after 50 min. For the adult OSA patients and healthy volunteers, two groups of three occlusions were induced at the start of the first and last 10 min of the study, with 3-min interval within each group. All occlusions lasted two consecutive breaths before releasing. A repeated study following the same procedure was performed on one adult healthy volunteer and one adolescent OSA, with an interval of 62 and 29 days between the original and repeated study, respectively.

Data Acquisition

Four axial slices were simultaneously excited based on the CAIPIRINHA technique.[48] To image N slices, N unique multi-band RF pulses are applied alternatively, as shown in Figure 2. The k^{th} pulse is designed such that the phase difference between signal from adjacent slices is $2\pi k/N$, $k \in [0, N-1]$. This creates a unique linear phase along the slice select direction. If Cartesian readouts were used this would result in a shift of individual slice images along the phase encoding direction. When combined with radial sampling, it leads to destructive interference for all slices with non-constant initial RF phases, which significantly reduces the total amount of inter-slice interference.[49] Each slice can be recovered by multiplying the acquired data with the conjugate of the excited phase for the specific slice.

To maximize signal destruction from other slices, it is desirable to have a uniform distributions of spokes excited by each radio-frequency (RF) pattern. Golden Angle (GA) view ordering[50] is known to produce almost uniform distribution for *all* spokes in an arbitrary temporal window. Here we adopted a modified GA radial trajectory view ordering, where the azimuthal angle increment is 111.25°/N for N-slice imaging. Now the spokes excited by *each* RF pattern proceed by GA. While still allowing retrospective temporal window size selection, this produces a more uniform distribution for spokes excited by each RF pattern compared with conventional GA. Figure 3 shows a representative frame of both conventional GA and modified GA sampling for four-slice imaging.

A custom-built radial grandient echo (GRE) pulse sequence was used to scan all subjects. Imaging parameters were: 5° flip angle, 200 samples per readout, field of view (FOV) $200 \times 200\,mm^2$, echo time/repetition time (TE/TR) 2.4/4 ms, $1 \times 1\,mm^2$ in-plane resolution. A fixed slice thickness/gap (7 mm/3 mm) were used, which led to three- or four-slice coverage from soft palate to epiglottis depending on the subject's pharyngeal airway length.

Reconstruction

Depending on the respiratory rate of each subject during the occlusion, 24–32 spokes were used to reconstruct one temporal frame, which led to 96–128 ms temporal resolution. The specific temporal resolution was retrospectively chosen such that at least 20 frames were acquired per occluded breath. Non-Cartesian SENSE[51] and compressed sensing with temporal finite difference

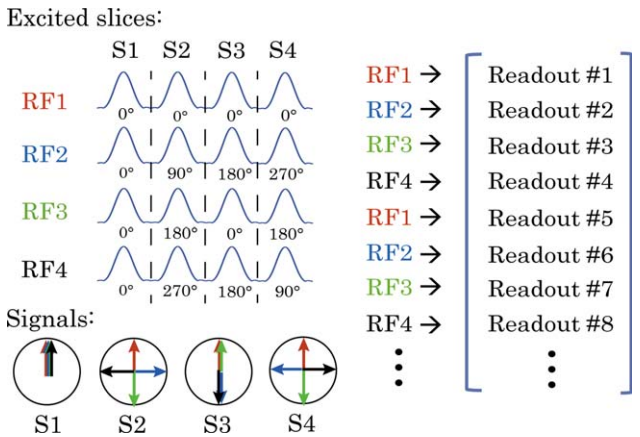

FIGURE 2: CAIPIRINHA excitation. Illustration of four-slice SMS excitation for CAIPIRINHA. In general, for N slices, N unique multi-band RF pulses are applied alternatively. The k^{th} pulse generates a transverse phase difference between adjacent slices of $2\pi k/N$, $k \in [0, N-1]$. When combined with radial sampling, this leads to signal destructive interference for all slices with noncompensated RF phase (by means of conjugate phase reconstruction).

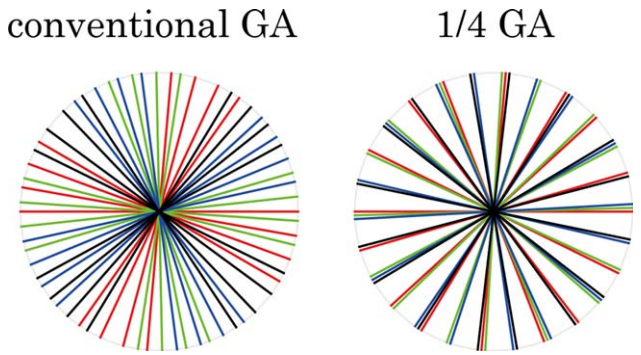

FIGURE 3: Modified GA sampling. One representative temporal frame with 32 spokes, for (left) conventional GA and (right) modified GA sampling trajectories for 4-slice CAIPIRINHA excitation. Spoke colors correspond to their excitation RF pulses in Figure 2. The modified method provides a more uniform distribution of spokes excited by *each* RF pattern. After gridding, this leads to better cancellation of signals from slices other than the one to be preserved at the more densely sampled k-space center.

as the sparsity constraint[52] was used to reconstruct each slice separately by iteratively minimizing the cost function:

$$f_i = \sum_j ||ES_{ij}m_i - P_i k_j||_2^2 + \lambda_i ||\phi m_i||_1, \quad i \in [1, N], \ j \in [1, Nc]$$

where i and j are the slice and coil index, respectively, P_i is the conjugate of the RF phase cycling pattern for slice i, E is the inverse gridding operator, S_{ij} is the coil sensitivity map for coil j and slice i, k_j is the acquired k-space data from coil j, ϕ is the finite temporal difference, and m_i is the individual slice image to be solved. m_i was initialized as $m_i^{(0)} = \sum_j S_{ij}E^H P_i k_j$, where E^H is the gridding operator. The regularization factor λ_i was empirically set to be 1/4 of the maximum intensity of slice i after initialization ($m_i^{(0)}$).

The first term in the above equation is a data consistency term for slice i. The second term enforces sparsity by minimizing the l_1-norm of the temporal finite difference of m_i. A nonlinear conjugate gradient approach was adopted to minimize the cost function during the optimization process, as described in the Appendix in Lustig et al.[53] In this study, the reconstruction time for scan segments of 10–20 s (100–200 frames) was 10–30 min per slice on a Linux workstation with 2.93 GHz CPU and 96 GB memory.

Postprocessing

The airway was segmented in each frame using a semi-automated region-growing algorithm.[44] Two seeds were manually put inside the airway in the first frame for dynamic series. The algorithm then automatically generated the segmented airways for all the temporal frames. For each subject, the airway area was normalized by the maximum cross-sectional area among all slices during tidal breathing to facilitate inter-subject comparison. Each of the two breath within one occlusion was further divided into the inhale portion and exhale potion and a linear regression (airway area versus pressure) was performed for each portion, from which the compliance (line slope) and the linearly projected closing pressure P_{close} (horizontal zero-crossing) were calculated. The unit for compliance in this work is cm H_2O^{-1} (normalized area / pressure), and the unit for P_{close} is cm H_2O.

Data Analysis

All slices were grouped into the retropalatal and retroglossal regions. For the adolescent OSA patients, three of the five adolescent OSA patients fell asleep within 1 h. Compliance and P_{close} of the corresponding inhale/exhale portion and breath within one occlusion were averaged over the three occlusions during sleep (if available), and averaged over the two groups of three occlusions during wakefulness in each region of all the subjects. To quantify the muscle tone's effect on airway collapsibility, paired Student's t-tests were performed between the inhale portion of the first breath and all the inhale/exhale portions of the two breaths within each occlusion, during sleep and wakefulness, respectively.

Airway collapsibility was also compared across different subject categories. To remove the impact of muscle tone change among different subjects as much as possible, only data from the inhale portion of the first breath within each of the six occlusions during wakefulness were used for inter-subject averaging and inter-category comparison. The compliance and P_{close} from the adolescent OSA and adult OSA groups were compared against the adult control, using Student's t-test and *P*-values were calculated.

To quantify the uniformity of airway collapse, the airway diameters in the left–right and anterior–posterior direction were measured in the temporal frames with the largest and smallest segmented airway areas in the retropalatal and retroglossal regions, respectively, for each subject. The ratio of the diameter difference in the two directions were averaged over all subjects within different categories. Paired Student's t-tests were performed between the adolescent/adult OSA groups and the adult control, as well as between the retropalatal and retroglossal regions within each subject group.

The compliance and P_{close} values were compared between the original and repeated study of the adult healthy volunteer and the adolescent OSA patient, respectively, also using Student's t-test.

Results

Figures (4 and 5) contain representative results from one adolescent OSA patient during sleep using four-slice acquisition. In Figure 4, the location of acquired slices are shown in the sagittal view. The top row on the right shows one frame at these locations when the airway was open during tidal breathing. The second row shows another frame when the airway was partially collapsed during one occluded breath. The bottom two rows show the segmented airways in enlarged views. Figure 5a shows the cross-sectional area of each slice together synchronized with the mask pressure during the occluded breath. The shaded area represents the inhale potion of the first occluded breath. Figure 5b shows the linear regression results for each of the four slices using data from the shaded area. The R^2 values were 0.94, 0.95, 0.94, 0.91, for slice 1–4, respectively. Note that although slice 1 (red) was not the narrowest during steady state (pressure = 0 cm H_2O), it was the most collapsible site based on

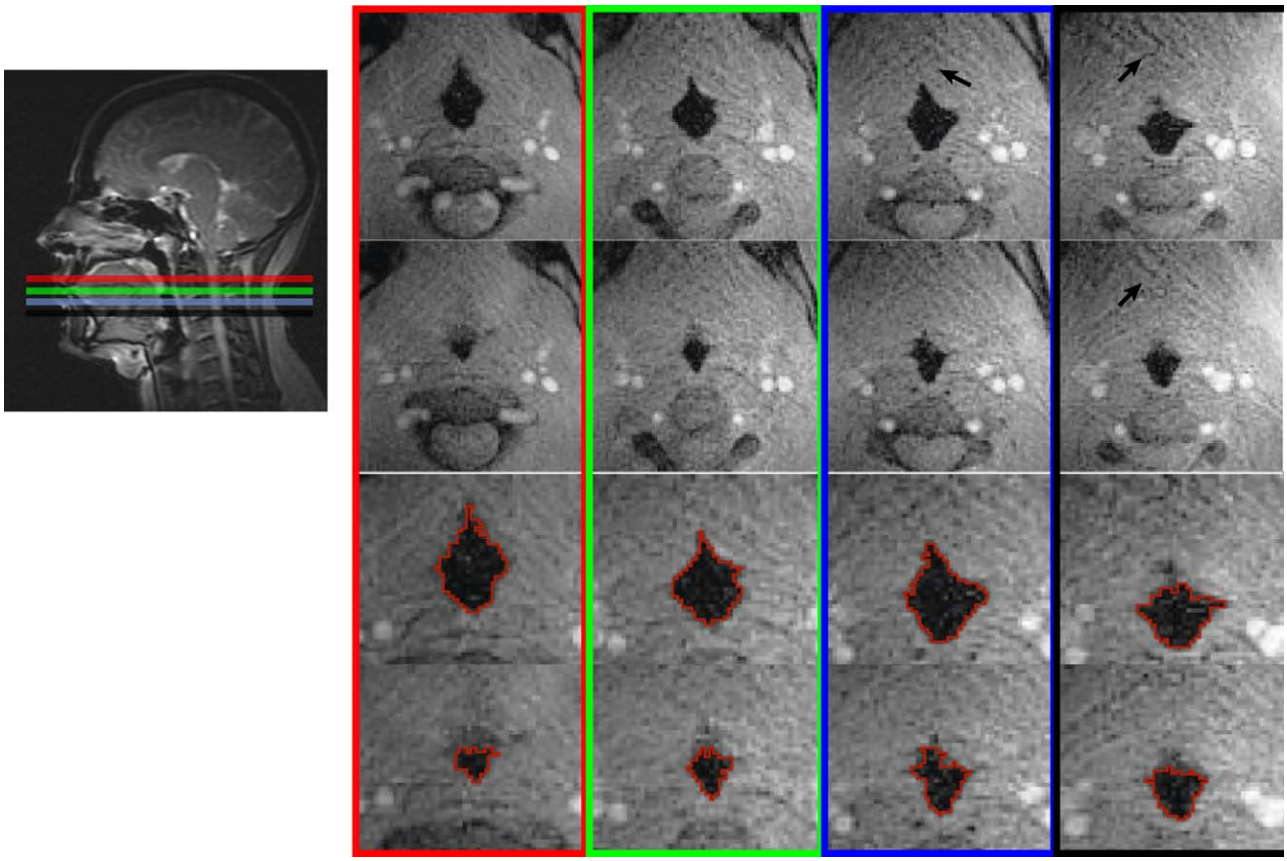

FIGURE 4: Representative frames from one sleep apnea patient. Four-slice SMS acquisition covering from soft palate to epiglottis were used, as shown in the sagittal view. Top row: One frame when the airways are open during tidal breathing. Second row: one frame when the airways are partially collapsed. The bottom two rows show the enlarged airways with segmentation. There is a 42–79% airway cross-sectional area change due to the inspirational load at different locations. Note that residual streaking artifacts (black arrows) can be observed due to heavy undersampling; however, they have negligible impact on airway boundary depiction.

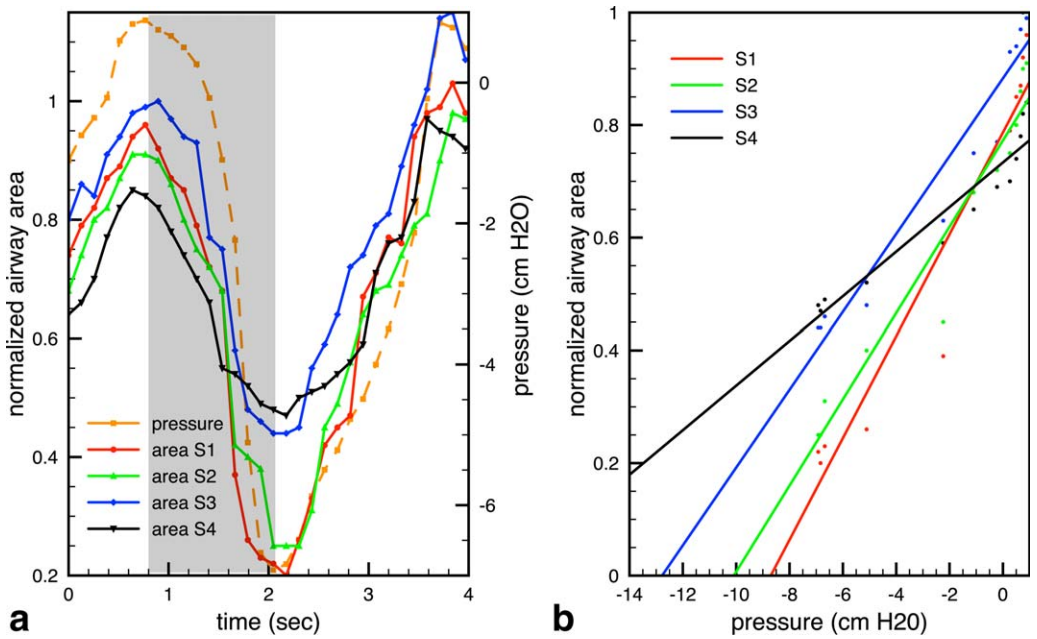

FIGURE 5: Compliance and projected closing pressure (P_{close}) Calculation. a: Cross-sectional area of the patent airway in each slice and the facemask pressure during one representative occluded breath. b: Linear regression of data from the inhale portion (shaded area in a), from which the compliance (slope) and P_{close} (x-intercept) values are calculated. Colors correspond to the slice locations in Figure 4. Note that slice 4 is the narrowest at baseline, whereas slice 1 is the most compliant and has the highest P_{close}, suggesting that it is the more likely point of collapse.

TABLE 1. Comparison of Compliance and P_{close} among Inhalation and Exhalation of Different Breaths during Sleep[a]

	Retropalatal		Retroglossal	
	Compliance (*P*-value)	**P_{close}(*P*-value)**	**Compliance (*P*-value)**	**P_{close}(*P*-value)**
Breath 1 inhale	.095±.024 (1.000)	−9.06 ± 2.27 (1.000)	.085±.015 (1.000)	−11.18 ± 2.03 (1.000)
Breath 1 exhale	.098±.014 (0.609)	−9.21 ± 1.95 (0.533)	.084±.020 (0.295)	−11.42 ± 2.53 (0.652)
Breath 2 inhale	.103±.019 (0.162)	−8.57 ± 1.73 (0.119)	.090±.017 (0.183)	−10.74 ± 2.21 (0.287)
Breath 2 exhale	.101±.022 (0.313)	−8.69 ± 1.50 (0.137)	.088±.013 (0.510)	−10.99 ± 2.27 (0.343)

[a]Data from the first two consecutive breaths within one occlusion were used. Each breath was further divided into the inhale portion and exhale potion. Each listed mean ± SD of compliance and P_{close} was calculated using data from the corresponding portion and breath only, from a total of 3 (subjects) × 2 (slices) × 3 (occlusions) = 18 occlusions. All data were acquired from the adolescent OSA patients during sleep (two subjects who did not fall asleep were excluded). In each column, the p-values were calculated against the inhale portion of breath 1. The unit for compliance is cm H_2O^{-1} (normalized area / pressure), and the unit for P_{close} is cm H_2O.

compliance and P_{close}. In contrast, slice 4 had the narrowest airway area during steady state, but was the least collapsible site.

Table 1 and Table 2 list the compliance and P_{close} values among the inhale/exhale portions of the two breaths within one occlusion, during sleep and wakefulness, respectively. Only adolescent OSA patients data were used, as mentioned in the Data Analysis section. In each column, the *P*-values were calculated against the inhale portion of breath 1. Note that most of the *P*-values in Table 2 were at least two magnitudes lower than the corresponding ones in Table 1. This indicates that the change of both compliance and P_{close} between the inhale portion of breath 1 and subsequent portions were more significant during wakefulness ($P < 0.01$) than during sleep ($P > 0.1$).

Table 3 compares the compliance and P_{close} values among the three subject groups during wakefulness. There was a significant difference of compliance and P_{close} between the OSA (adolescent and adult) patients and healthy adult controls ($P < 0.001$). Within each group, the region-wise Student's t-test suggests that adolescent OSA patients had a noticeably higher compliance and P_{close} in the retropalatal region compared with the retroglossal region ($P < 0.001$). This regional variation was insignificant in both adult OSA and control groups ($P > 0.1$).

Table 4 shows the ratio of the maximal airway change in the right–left (RL) direction and anterior–posterior (A-P) direction. A ratio higher than 1 indicates the airway collapses more easily in the RL direction than AP direction. The mean values of the ratio were close to 1 in all cases, except in the retropalatal region of the adolescent OSA group (1.42), suggesting the airways tend to be more collapsible in the RL direction in such case. When compared with the adult control group using Student's t-test (the first two columns), it also shows that only the retropalatal region of the adolescent OSA group was significantly different from the

TABLE 2. Comparison of Compliance and P_{close} among inhaLation and Exhalation of Different Breaths during Wakefulness[a]

	Retropalatal		Retroglossal	
	Compliance (*P*-value)	**P_{close}(*P*-value)**	**Compliance (*P*-value)**	**P_{close}(*P*-value)**
Breath 1 inhale	.087±.021 (1.000)	−10.13 ± 2.54 (1.000)	.077±.019 (1.000)	−13.25 ± 2.91 (1.000)
Breath 1 exhale	.106±.016 (1×10^{-4})	−8.81 ± 1.74 (7×10^{-4})	.080±.013 (0.002)	−11.42 ± 1.85 (2×10^{-4})
Breath 2 inhale	.081±.027 (6×10^{-4})	−11.24 ± 2.88 (0.006)	.068±.015 (0.004)	−14.35 ± 2.16 (0.004)
Breath 2 exhale	.092±.029 (5×10^{-4})	−9.98 ± 3.07 (0.003)	.075±.017 (0.009)	−12.73 ± 2.77 (0.007)

[a]Each listed mean ± SD of compliance and P_{close} was calculated exactly the same as in Table 1, except from a total of 5 (subjects) x 2 (slices) x 6 (occlusions) = 60 occlusions. Two groups of three occlusions were induced at the first and last 10 min of the 1-h study, respectively, while the adolescent OSA patients were awake. For each column, the *P*-values were calculated against the inhale portion of breath 1.

TABLE 3. Comparison of Compliance and P_{close} among Different Subject Groups[a]

	Retropalatal		Retroglossal		Region-wise comparison (retropalatal versus retroglossal)	
	Compliance (p-value)	P_{close}(p-value)	Compliance (p-value)	P_{close}(p-value)	Compliance	P_{close}
Adult control	.042±.012 (1.000)	−24.18 ± 5.14 (1.000)	.039±.008 (1.000)	−25.94 ± 5.45 (1.000)	0.217	0.207
Adolescent OSA	.087±.021 (3×10^{-25})	−10.13 ± 2.54 (1×10^{-30})	.077±.019 (1×10^{-25})	−13.25 ± 2.91 (1×10^{-23})	8×10^{-5}	5×10^{-18}
Adult OSA	.072±.018 (9×10^{-18})	−13.23 ± 3.77 (9×10^{-18})	.070±.016 (1×10^{-21})	−14.31 ± 3.33 (3×10^{-16})	0.189	0.318

[a]Each listed mean ± SD of compliance and P_{close} was calculated from all available data during wakefulness, using the inhale portion of the first occluded breath only. There were four/five/three subjects in adult control, adolescent OSA, adult OSA group, and two slices per retropalatal and retroglossal region, respectively. Each subject had a total of six occlusions during wakefulness. The *P*-values in the first four columns were computed against the adult control group. The last two columns show the *P*-values when comparing the retropalatal region with the retroglossal region.

same region in adult controls ($P < 0.001$). The region-wise comparison within each group (last column) indicates that the adult OSA and adolescent OSA groups exhibited a significant difference of the directional collapsibility in the retropalatal and retroglossal region ($P < 0.001$), while the adult control group did not ($P > 0.01$).

Table 5 lists the test–retest comparisons of the compliance and P_{close} values for the two subjects who had repeated studies. The *P*-values were higher than 0.1 in almost all cases, except the P_{close} of the retroglossal region (adolescent OSA), which was very close to 0.1 ($P = 0.098$). It indicates that the measurement variations were insignificant between the original and repeated study for both subjects.

Discussion

We show that SMS real-time MRI can provide valuable information to help diagnosing sleep apnea in addition to PSG. In our experience, OSA patients typically have small airways and insufficient spatial resolution (> 1 mm) may introduce obvious partial volume artifacts. It also requires a few temporal frames with more negative pressures ($<$ -3 cm H_2O) to make the linear regression robust. But these frames are difficult to capture with insufficient temporal resolution (< 100 ms). More spatial coverage than a single slice is also useful because airway collapsibility varies at different axial locations. Therefore, it is essential to achieve the spatial coverage from soft palate to epiglottis and the 1 mm/ 100 ms spatiotemporal resolution target[43] at the same time. When compared with previous works,[44–47] the proposed method is able to provide the desired spatiotemporal resolution and spatial coverage at the same time for the evaluation of upper airway collapsibility. Here, we report several interesting findings.

The proposed reconstruction is able to recover the relevant airway boundary information. Minor residual streaking artifacts persists but does not affect airway segmentation. This may be mitigated by sacrificing temporal resolution. However, we purposely chose a high temporal resolution (~100 ms) because it is critical to fully resolve the airway dynamics. Both the compliance and P_{close} values vary among different slices, which confirms the value of simultaneous multi-slice imaging.

One important finding is that a narrower airway site during tidal breathing does not necessarily have higher compliance or P_{close}, and, therefore, is not always the most collapsible. Vice versa, the most collapsible airway site is not necessarily the narrowest during tidal breathing. We observed this phenomenon in approximately half of the subjects studied (2/5 adolescent OSA, 1/3 adult OSA, 2/4 adult healthy control). To the best of our knowledge, this is the first time that this finding has been discovered experimentally. Currently, for OSA patients who cannot tolerate CPAP treatment and seek sleep surgeries, the success rate is only approximately 60% in the short term (3–6 months) and can degrade to $< 50\%$ in the long-term.[54] Some

TABLE 4. Ratio of the Maximal Airway Change in the Right–Left Direction and Anterior–Posterior Direction[a]

	Retropalatal	Retroglossal	Region-wise comparison
	RL/AP (p-value)	RL/AP (p-value)	
Adult control	1.13 ± 0.18 (1.000)	1.05 ± 0.07 (1.000)	0.011
Adolescent OSA	1.42 ± 0.27 (1×10^{-6})	1.12 ± 0.15 (0.003)	7×10^{-7}
Adult OSA	1.18 ± 0.35 (0.122)	0.93 ± 0.23 (0.168)	4×10^{-5}

[a]The ratio is a reflection of the uniformity of airway collapse. A ratio higher than 1 indicates the airway collapses more easily in the RL direction than AP direction. Each listed mean ± SD of the ratio was calculated from all available data during wakefulness, using the inhale portion of the first occluded breath only. There were four/three/five subjects in adult control, adolescent OSA, adult OSA group, and two slices per retropalatal and retroglossal region, respectively. Each subject had a total of six occlusions during wakefulness. The *P*-values in the first two columns were computed against the adult control group. The last column shows the *P*-values when comparing the retropalatal region with the retroglossal region within each group.

patients even have worse apnea after the surgeries. In these surgeries, excessive airway tissues are typically removed at the narrowest site without considering their collapsibility. Although drug-induced sleep endoscopy[26] has been used clinically to identify airway obstruction site, it requires anesthesia, which may not reflect the true tissue collapsibility. We hypothesize that our finding could be the reason why sleep surgeries have low success rate. The ability of the proposed method to identify the most collapsible site may help sleep surgeons identify the optimal location for intervention and potentially improve surgery success rate.

This study observed that compliance and P_{close} during sleep have smaller variance among the inhale/exhale portions of different breaths within one occlusion, when compared with wakefulness. This is likely due to the involuntary airway muscle tone change that prevents the airway from collapsing.[55] As a self-defense mechanism, the airway muscles will respond to the passive stretch induced by occlusion and become stiffer, in an effort to prevent the airway from collapsing. This response is much more obvious during wakefulness. Although ideally the airway collapsibility should be measured during sleep, it may not be feasible for several practical reasons. First, our experiment has several constraints such as a supine position, wearing a facemask, and MRI acoustic noise. Second, MRI scan time is expensive and falling asleep without sedation takes time and can be unpredictable. In this study, approximately half (3 of 5) adolescent OSA patients fell asleep within 1 h. Therefore, it may be more practical to perform the compliance test during wakefulness, which typically requires approximately 30 min total scan room time. Combining all the data of the two breaths within one occlusion will likely to make the compliance and P_{close} values corrupted by the muscle tone change. To minimize such bias, which can be very subject dependent, we propose to use only the inhale portion of the first occluded breath for inter-subject comparison. Under such conditions, it can still reflect the relative differences between the retropalatal and retroglossal regions. Although one should note that both compliance and P_{close} values are smaller than during sleep.

The difference of compliance and P_{close} values between the OSA (adolescent and adult) patients and healthy adult controls was significant. This suggests that both collapsibility measures can potentially serve as biomarkers for diagnosing

TABLE 5. Test-Retest Reproducibility Comparison[a]

		Retropalatal		Retroglossal	
		Compliance	P_{close}	Compliance	P_{close}
Adult volunteer	Study 1	.047±.007	-21.52 ± 1.53	.042±.005	-22.01 ± 1.76
	Study 2	.044±.009	-20.47 ± 1.97	.040±.004	-20.84 ± 1.99
	P-value	0.153	0.391	0.192	0.211
Adolescent OSA	Study 1	.075±.010	-11.33 ± 1.16	.068±.008	-14.01 ± 1.55
	Study 2	.079±.013	-10.92 ± 0.96	.069±.011	-14.58 ± 1.94
	P-value	0.663	0.221	0.576	0.098

[a]One adolescent OSA patient and one adult healthy volunteer had repeated studies on two different days (29-day interval for the patient and 62-day interval for the volunteer). The compliance and P_{close} were measured during wakefulness. *P*-values were calculated between the two studies for both subjects.

OSA. Another interesting finding is only in the adolescent OSA group, we can see a noticeably higher compliance and P_{close} in the retropalatal region compared with the retroglossal region. This is in consistent with Schwab et al,[56] in which the retropalatal region is also recommended for initial treatment consideration for adolescent based on a large population study. This regional variation is not observed in both adult OSA and control groups.

The airways tend to be more collapsible in the RL direction than AP direction in the retropalatal region of the adolescent OSA patients only. This is likely due to the enlarged tonsils commonly found in OSA patients. A less obvious difference can be observed in the adult OSA group. We do not know the precise reason based on the limited data. But we hypothesize this could be due to the adapted muscle tone change over time to prevent the airway from collapsing in the adult OSA group. This change may be more drastic in the tissues that were previously easier to collapse, so that the collapse becomes more uniform overall.

The measurement variations between the two repeated studies of both the adult volunteer and the adolescent OSA patient were relatively small and within reasonable range, given the possible change of airway collapsibility over the 62/29 days and/or the conditions on the study days. Although it requires more subjects to fully demonstrate the test–retest reproducibility, we believe the study results are repeatable based on the test–retest results from these two subjects.

This study has several limitations. First, we had a small sample size ($N = 12$). The findings and implications discussed above require experimental confirmation in a larger cohort. Second, our goal here is to identify new image-based biomarkers enabled by modern real-time MRI methods. We did not experimentally optimize the real-time MRI parameters, specifically the trade-offs between slice coverage (slice numbers, thickness, and gap), spatiotemporal resolution, and regularization. This optimal choice of these parameters requires additional investigation. Third, reconstruction was not performed in real-time. With optimization of the reconstruction implementation, including the use of parallel computing, reconstruction time can be significantly improved, and remains as future work. Finally, the airway segmentation software we used has not been validated against Radiologists' manual segmentation. We had to manually adjust the segmentation in a small number of cases due to through plane movement of the soft palate. More sophisticated segmentation methods will likely improve the accuracy and reduce the need for manual intervention.

In conclusion, we have demonstrated a novel imaging method for airway compliance measurement that uses an inspiratory load and SMS RT-MRI. It combines several acceleration techniques including SMS, parallel imaging, modified GA radial trajectory, and compressed sensing, to achieve 33.3 times acceleration compared with fully sampled Cartesian scanning. We have also experimentally discovered that a narrower airway site does not always correspond to higher collapsibility. This finding may be of interest to sleep surgeons. Our preliminary results suggest that both compliance and P_{close}, as measured by SMS real-time MRI, may serve as biomarkers to diagnose OSA, and can be calculated with a 20-s awake scan. Even with experiment setup time and a few repeated measurements for sanity check, it should take less than 30 min total scan room time.

Acknowledgments

Contract grant sponsor: NIH; contract grant number: R01-HL105210

References

1. Strollo PJ, Rogers RM. Obstructive sleep apnea. N Engl J Med 1996; 334:99–104.
2. Javaheri S, Parker TJ, Liming JD, Corbett WS, Nishiyama H, Wexler L, et al. Sleep apnea in 81 ambulatory male patients with stable heart failure types and their prevalences, consequences, and presentations. Circulation 1998;97:2154–2159.
3. Bassetti CL, Milanova M, Gugger M. Sleep-disordered breathing and acute ischemic stroke diagnosis, risk factors, treatment, evolution, and long-term clinical outcome. Stroke 2006;37:967–972.
4. Vgontzas AN, Tan TL, Bixler EO, Martin LF, Shubert D, Kales A. SLeep apnea and sleep disruption in obese patients. Arch Intern Med 1994; 154:1705–1711.
5. Tasali E, Mokhlesi B, Van Cauter E. Obstructive sleep apnea and type 2 diabetes*: interacting epidemics. Chest 2008;133:496–506.
6. The Price of Fatigue: the surprising economic costs of unmanaged sleep apnea. Cambridge, MA: Harvard Medical School; 2010.
7. Sforza E, Bacon W, Weiss T, Thibault A, Petiau C, Krieger J. Upper airway collapsibility and cephalometric variables in patients with obstructive sleep apnea. Am J Respir Crit Care Med 2000;161:347–352.
8. Malhotra A, Pillar G, Fogel R, Beauregard J, Edwards J, White DP. Upper-airway collapsibility*: measurements and sleep effects. Chest 2001;120:156–161.
9. Schwartz AR, Patil SP, Laffan AM, Polotsky V, Schneider H, Smith PL. Obesity and obstructive sleep apnea. Proc Am Thorac Soc 2008;5: 185–192.
10. Arens R, Marcus CL. Pathophysiology of upper airway obstruction: a developmental perspective. Sleep 2004;27:997–1019.
11. James PT, Leach R, Kalamara E, Shayeghi M. The worldwide obesity epidemic. Obes Res 2001;9:228–233.
12. Practice parameters for the indications for polysomnography and related procedures. Polysomnography Task Force, American Sleep Disorders Association Standards of Practice Committee. Sleep 1997; 20:406–422.
13. Kushida CA, Littner MR, Morgenthaler T, Alessi CA, Bailey D, Coleman J, et al. Practice parameters for the indications for polysomnography and related procedures: an update for 2005. Sleep 2005;28:499–521.
14. Sleep-related breathing disorders in adults: recommendations for syndrome definition and measurement techniques in clinical research. The Report of an American Academy of Sleep Medicine Task Force. Sleep 1999;22:667–689.

15. Ruehland WR, Rochford PD, O'Donoghue FJ, Pierce RJ, Singh P, Thornton AT. The New AASM criteria for scoring hypopneas: impact on the apnea hypopnea index. Sleep 2009;32:150–157.

16. Punjabi NM. The epidemiology of adult obstructive sleep apnea. Proc Am Thorac Soc 2008;5:136–143.

17. Gozal D. Obstructive sleep apnea in children: implications for the developing central nervous system. Semin Pediatr Neurol 2008;15: 100–106.

18. Marcus CL, McColley SA, Carroll JL, Loughlin GM, Smith PL, Schwartz AR. Upper airway collapsibility in children with obstructive sleep apnea syndrome. J Appl Physiol 1994;77:918–924.

19. White DP. Pathogenesis of obstructive and central sleep apnea. Am J Respir Crit Care Med 2005;172:1363–1370.

20. Slaats MA, Van Hoorenbeeck K, Van Eyck A, Vos WG, De Backer JW, Boudewyns A, et al. Upper airway imaging in pediatric obstructive sleep apnea syndrome. Sleep Med Rev 2015;21:59–71.

21. Barrera JE. Sleep magnetic resonance imaging: dynamic characteristics of the airway during sleep in obstructive sleep apnea syndrome. Laryngoscope 2011;121:1327–1335.

22. Donnelly LF, Strife JL, Myer CM. Dynamic sleep fluoroscopy in children with obstructive sleep apnea. Appl Radiol 2001;30:30–34.

23. Brouillette RT, Fernbach SK, Hunt CE. Obstructive sleep apnea in infants and children. J Pediatr 1982;100:31–40.

24. Isono S, Shimada A, Tanaka A, Tagaito Y, Utsugi M, Konno A, et al. Efficacy of endoscopic static pressure/area assessment of the passive pharynx in predicting uvulopalatopharyngoplasty outcomes. Laryngoscope 1999;109:769–774.

25. Ng AT, Qian J, Cistulli PA. Oropharyngeal collapse predicts treatment response with oral appliance therapy in obstructive sleep apnea. Sleep 2006;29:666–671.

26. Kezirian EJ. Drug-induced sleep endoscopy. Oper Tech Otolaryngol-Head Neck Surg 2006;17:230–232.

27. Stein M, Gamsu G, de Geer G, Golden J, Crumley R, Webb W. Cine CT in obstructive sleep apnea. AJR Am J Roentgenol 1987;148:1069–1074.

28. Shepard JW Jr, Stanson AW, Sheedy PF, Westbrook PR. Fast-CT evaluation of the upper airway during wakefulness in patients with obstructive sleep apnea. Prog Clin Biol Res 1990;345:273–279.

29. Schwab RJ, Gefter WB, Hoffman EA, Gupta KB, Pack AI. Dynamic upper airway imaging during awake respiration in normal subjects and patients with sleep disordered breathing. Am Rev Respir Dis 1993;148:1385–1400.

30. Brooks LJ, Byard PJ, Fouke JM, Strohl KP. Reproducibility of measurements of upper airway area by acoustic reflection. J Appl Physiol 1989;66:2901–2905.

31. Huang J, Itai N, Hoshiba T, Fukunaga T, Yamanouchi K, Toga H, et al. A new nasal acoustic reflection technique to estimate pharyngeal cross-sectional area during sleep. J Appl Physiol 2000;88:1457–1466.

32. Jing J, Zhang J, Loy AC, Wong BJF, Chen Z. High-speed upper-airway imaging using full-range optical coherence tomography. J Biomed Opt 2012;17:110507.

33. Schwab RJ, Pasirstein M, Pierson R, Mackley A, Hachadoorian R, Arens R, et al. Identification of upper airway anatomic risk factors for obstructive sleep apnea with volumetric magnetic resonance imaging. Am J Respir Crit Care Med 2003;168:522–530.

34. Arens R, McDonough JM, Costarino AT, Mahboubi S, Tayag-Kier CE, Maislin G, et al. Magnetic resonance imaging of the upper airway structure of children with obstructive sleep apnea syndrome. Am J Respir Crit Care Med 2001;164:698–703.

35. Donnelly LF, Surdulescu V, Chini BA, Casper KA, Poe SA, Amin RS. Upper airway motion depicted at cine MR imaging performed during sleep: comparison between young patients with and those without obstructive sleep apnea. Radiology 2003;227:239–245.

36. Arens R, Sin S, McDonough JM, Palmer JM, Dominguez T, Meyer H, et al. Changes in upper airway size during tidal breathing in children with obstructive sleep apnea syndrome. Am J Respir Crit Care Med 2005;171:1298–1304.

37. Donnelly LF. Obstructive sleep apnea in pediatric patients: evaluation with cine MR sleep studies. Radiology 2005;236:768–778.

38. Wagshul ME, Sin S, Lipton ML, Shifteh K, Arens R. Novel retrospective, respiratory-gating method enables 3D, high resolution, dynamic imaging of the upper airway during tidal breathing. Magn Reson Med 2013;70:1580–1590.

39. Issa FG, Sullivan CE. Upper airway closing pressures in obstructive sleep apnea. J Appl Physiol 1984;57:520–527.

40. Isono S, Morrison DL, Launois SH, Feroah TR, Whitelaw WA, Remmers JE. Static mechanics of the velopharynx of patients with obstructive sleep apnea. J Appl Physiol 1993;75:148–154.

41. Isono S, Remmers JE, Tanaka A, Sho Y, Sato J, Nishino T. Anatomy of pharynx in patients with obstructive sleep apnea and in normal subjects. J Appl Physiol 1997;82:1319–1326.

42. Ryan CM, Bradley TD. Pathogenesis of obstructive sleep apnea. J Appl Physiol 2005;99:2440–2450.

43. Nayak KS, Fleck RJ. Seeing sleep: dynamic imaging of upper airway collapse and collapsibility in children. Pulse IEEE 2014;5:40–44.

44. Kim Y-C, Wang X, Tran W, Khoo MC, Nayak KS. Measurement of upper airway compliance using dynamic MRI. In: Proceedings of the 20th Annual Meeting of ISMRM, Melbourne, Australia, 2012.

45. Colrain I, Nayak K, Nielsen J. Real-time MRI of upper airway collapse during inspiratory loading. In: Proceedings of the 14th Annual Meeting of ISMRM, Seattle, 2006.

46. Shin LK, Holbrook AB, Capasso R, Kushida CA, Powell NB, Fischbein NJ, et al. Improved sleep MRI at 3 tesla in patients with obstructive sleep apnea. J Magn Reson Imaging 2013;38:1261–1266.

47. Kim Y-C, Lebel RM, Wu Z, Ward SLD, Khoo MCK, Nayak KS. Real-time 3D magnetic resonance imaging of the pharyngeal airway in sleep apnea. Magn Reson Med 2014;71:1501–1510.

48. Breuer FA, Blaimer M, Heidemann RM, Mueller MF, Griswold MA, Jakob PM. Controlled aliasing in parallel imaging results in higher acceleration (CAIPIRINHA) for multi-slice imaging. Magn Reson Med 2005;53:684–691.

49. Yutzy SR, Seiberlich N, Duerk JL, Griswold MA. Improvements in multislice parallel imaging using radial CAIPIRINHA. Magn Reson Med 2011;65:1630–1637.

50. Winkelmann S, Schaeffter T, Koehler T, Eggers H, Doessel O. An optimal radial profile order based on the golden ratio for time-resolved MRI. IEEE Trans Med Imaging 2007;26:68–76.

51. Pruessmann KP, Weiger M, Bornert P, Boesiger P. Advances in sensitivity encoding with arbitrary k-space trajectories. Magn Reson Med 2001;46:638–651.

52. Feng L, Grimm R, Block KT, Chandarana H, Kim S, Xu J, et al. Golden-angle radial sparse parallel MRI: combination of compressed sensing, parallel imaging, and golden-angle radial sampling for fast and flexible dynamic volumetric MRI. Magn Reson Med 2014;72:707–717.

53. Lustig M, Donoho D, Pauly JM. Sparse MRI: the application of compressed sensing for rapid MR imaging. Magn Reson Med 2007;58: 1182–1195.

54. Sher AE. Upper airway surgery for obstructive sleep apnea. Sleep Med Rev 2002;6:195–212.

55. Remmers JE, deGroot WJ, Sauerland EK, Anch AM. Pathogenesis of upper airway occlusion during sleep. J Appl Physiol 1978;44:931–938.

56. Schwab RJ, Kim C, Bagchi S, Keenan BT, Comyn F-L, Wang S, et al. Understanding the Anatomic Basis for Obstructive Sleep Apnea Syndrome in Adolescents. Am J Respir Crit Care Med 2015;191:1295–1309.